

# The influence of carbon nanotubes, organically modified montmorillonites and layered double hydroxides on the thermal degradation and fire retardancy of polyethylene, ethylene–vinyl acetate copolymer and polystyrene

Marius C. Costache<sup>a</sup>, Matthew J. Heidecker<sup>b</sup>, E. Manias<sup>b</sup>, Giovanni Camino<sup>c</sup>,  
Alberto Frache<sup>c</sup>, Gunter Beyer<sup>d</sup>, Rakesh K. Gupta<sup>e</sup>, Charles A. Wilkie<sup>a,\*</sup>

<sup>a</sup> Department of Chemistry, Marquette University, P.O. Box 1881, Milwaukee, WI 53201, USA

<sup>b</sup> Department of Materials Science and Engineering, Penn State University, 325-D Steidle Bldg, University Park, PA 16802, USA

<sup>c</sup> Centro di Cultura per l'Ingegneria delle Materie Plastiche clo Politecnico di Torino sede di Alessandria, Viale Teresa Michel, 5 – 15100 Alessandria, Italy

<sup>d</sup> Kabelwerk Eupen AG, Malmeyer Strasse 9, B-4700 Eupen, Belgium

<sup>e</sup> Department of Chemical Engineering, West Virginia University, P.O. Box 6102, Morgantown, WV 26506, USA

Received 8 August 2007; received in revised form 20 August 2007; accepted 25 August 2007

Available online 1 September 2007

---

## Abstract

Nanocomposites of polyethylene, ethylene–vinyl acetate copolymer and polystyrene with single- and multi-wall carbon nanotubes, organically modified montmorillonites and layered double hydroxides were prepared by melt blending. Their morphologies were assessed by X-ray diffraction and transmission electron microscopy, while the flammability properties were evaluated by thermogravimetric analysis and cone calorimetry. The relative amounts and the identity of the degradation products are changed when both well-dispersed cationic and anionic clays are used, but there is no difference in the degradation products when carbon nanotubes were utilized. When the nano-dimensional material is not well-dispersed, the degradation products are not changed. Unlike their smectite counterparts, polymer/layered double hydroxide nanocomposites give reasonably good reductions in peak heat release even when good nano-dispersion has not been obtained. These data suggest that the enhancement in the fire behavior must be, at least in part, due to different mechanisms for montmorillonite, layered double hydroxides and carbon nanotube-based nanocomposites.

© 2007 Elsevier Ltd. All rights reserved.

*Keywords:* Nanocomposites; Mechanism; Thermal degradation

---

## 1. Introduction

Dispersion at a nanoscale of organically modified clays in polymers is well-known to enhance the mechanical, barrier, flammability properties as well as the thermal stability of the polymer matrix, even at low loadings (typically less than 10%) [1–6]. Enhanced fire retardancy has also been observed upon addition of other classes of fillers, such as layered double

hydroxides (LDHs) [7,8] and multi- or single-wall carbon nanotubes (CNTs) [9–13].

The single most used technique for characterization of flammability properties of polymer nanocomposites is cone calorimetry and the most informative property used for assessing the fire retardancy by this technique is the peak heat release rate (PHRR). The widely accepted mechanism to explain the reduction of PHRR is the barrier effect [14,15] due to clay platelets, according to which the clay layers slow both the mass and the heat transfer from and to the polymer.

---

\* Corresponding author.

E-mail address: [charles.wilkie@marquette.edu](mailto:charles.wilkie@marquette.edu) (C.A. Wilkie).

Recent work from this laboratory showed that for the polymers that exhibit a large reduction in PHRR upon nanocomposite formation using montmorillonite (MMT) as the nano-dimensional material, such as polystyrene (PS), polyamide-6 (PA-6) and ethylene–vinyl acetate copolymer (EVA), a change in the amounts and/or identity of the thermal degradation products occurs [16–18]. This change has been ascribed to secondary reactions (hydrogen abstraction, radical recombination reaction, extensive random scission, various intermolecular reactions, etc.) that can lead to new polymeric products which again must undergo thermal degradation. Radicals which have a substantial stabilization energy, *e.g.*, styryl radical from polystyrene or an allylic radical from EVA, will exist and be retained in the nanocomposite long enough to participate in additional reactions, while radicals which do not have this stabilization energy, *e.g.*, a methacrylate radical from poly(methyl methacrylate) [19] or a radical adjacent to a nitrile, from SAN [20], are not long lived and will not recombine [21].

Given the fact that the literature reports similar reductions in the peak heat release rate for other fillers [4,6] compared to montmorillonite-based polymer/clay nanocomposites, the question that logically arises is whether the smectite clays are unique or do other fillers, regardless of their chemical identity, have a similar effect on the degradation pathway of the polymer.

The thermal degradation of polystyrene (PS), ethylene–vinyl acetate (EVA) and polyethylene (PE) and has been extensively studied [22–29]. Degradation of PS proceeds by random scission followed by  $\beta$ -scission, leading to the formation of, mainly, monomer, dimer and trimer through intrachain reactions. In the case of EVA, thermal degradation proceeds in two steps. The first step is due to the loss of acetic acid by chain stripping and this leads to unsaturation and the formation of poly(ethylene-*co*-acetylene), which degrades in the second step. The second (main) degradation step is random scission of the backbone followed by radical transfer to the allylic position, whereupon either hydrogen loss or abstraction can lead to the formation of either an unsaturated or saturated chain end, respectively. Depending on what happens on the other end of the radical, the degradation products could be alkanes, terminal alkenes or  $\alpha,\omega$ -dienes [21]. The degradation of PE follows a similar mechanism as the main degradation of EVA, random scission, radical transfer and hydrogen loss/abstraction to generate the same hydrocarbon series (alkanes, alkenes or  $\alpha,\omega$ -dienes) [22] as from the main degradation step of EVA.

In this study, nanocomposites of polystyrene, polyethylene and ethylene–vinyl acetate copolymer were prepared using organically modified montmorillonite, organically modified layered double hydroxides, and single- and multi-wall carbon nanotubes as the nano-dimensional fillers. In addition to the standard morphological evaluation of the materials, fire properties were evaluated using cone calorimetry and the products of degradation were identified using TGA/FTIR and GC–MS techniques. Correlations between the identity and the amounts of the degradation products and the reduction in the peak heat

release rate were sought in order to evaluate the effects of the different nano-dimensional fillers on the degradation of the nanocomposites.

## 2. Experimental

### 2.1. Materials

Low density polyethylene (LDPE) with melt index 7 g/min (190 °C/2.16 kg) was used for the montmorillonite-based nanocomposites, polystyrene with average  $M_w \sim 230,000$ , average  $M_n \sim 140,000$ , softening point 107 °C (ASTM D 1525) and melt index 7.5 g/10 min (ASTM D 1238, 200 °C/5 kg), tetrahydrofuran (98%), benzoyl peroxide (97%), vinylbenzyl chloride (97%), styrene, lauryl acrylate, triethylamine, 10-undecenoic acid (98%), aluminum nitrate nanohydrate (98%), zinc nitrate hexahydrate (98%), sodium hydroxide and 2-amino-toluene-5-sulfonic acid (97%) were purchased from Aldrich Chemical Co., Inc. The LDPE used for the PE–CNT nanocomposites was BPD 8063 from BP Petrochemicals, while the medium density PE was purchased from Aldrich. Sodium montmorillonite and Cloisite 30B (a montmorillonite exchanged with methyl, tallow, bis-2-hydroxyethyl, quaternary ammonium; where tallow is a naturally derived alkyl containing a mixture of about 65%  $C_{18}H_{37}$ , 30%  $C_{16}H_{33}$ , and 5%  $C_{14}H_{29}$ ) were provided by Southern Clay Products. The ethylene–vinyl acetate copolymer used was Escorene Ultra LD 728 with 19 wt% vinyl acetate and melt flow index 2.0 g/10 min, produced and kindly provided by ExxonMobil Co. Multi-wall carbon nanotubes (MWCNTs) were kindly provided by Olivier Decroly, Nanocyl S.A., Belgium, while the organically modified layered double hydroxides used were derived from Pural MG63HT (magnesium–aluminum layered double hydroxide intercalated with carbonate anion), kindly provided by Sasol. The iron-free montmorillonite (sodium form) was Barasym SSM-100 and was purchased from the Clay Mineral Society. All of these were used without further purification. Many of the polyethylene nanocomposites used in this work have already been described in the literature and were kindly provided by those authors [4,6], where the morphological evaluation of those nanocomposites had not been reported, it is included in this work.

### 2.2. Instrumentation

Dispersion of silicates in the polymer matrix was observed by X-ray diffraction (XRD) measurements performed using a Rigaku powder diffractometer with a Cu source ( $\lambda = 1.54 \text{ \AA}$ ), scanning  $2\theta$  from 1° to 10°, at a 0.1° step size; generator tension was 50 kV at 20 mA.

The PE and EVA samples for TEM were prepared by cryo sectioning in a RMR Powertome XL Ultramicrotome using a diamond knife. The samples were sectioned at –125 °C in the case of PE blends and at –60 °C in the case of EVA blends. The thin sections were stained with ruthenium tetroxide vapors (freshly prepared) before examining in a JEOL 100CX transmission electron microscope operated at accelerating

voltage of 100 kV. For the polystyrene nanocomposites, bright field TEM images were obtained with a JEOL 1200 EXII microscope operated with an accelerating voltage of 80 kV, and equipped with a Tietz F224 digital camera. Thin sections of the nanocomposites were cut from a plaque using a microtome (Leica Ultracut UCT) equipped with a diamond knife. The sections were transferred to carbon-coated copper grids (200-mesh). No heavy metal staining of sections prior to imaging was necessary for the PS samples.

TGA/FTIR was performed in quartz pans in nitrogen, at a flow rate of 60 ml/min and a heating rate of 20 °C/min on a Cahn TG 131 instrument connected to a Mattson Research grade FTIR. The evolved volatile products were sampled at a rate of 40 ml/min, using a 'sniffer' tube that extended to the sample cup. The evolved gases were carried through stainless steel tubing to the IR chamber, the temperature of the tubing and the sample cell was maintained at 250–300 °C. The sample size is 40–60 mg and the temperature reproducibility of the TGA is  $\pm 3$  °C while the fraction of non-volatile is  $\pm 3\%$ .

Cone calorimetric measurements were performed at an incident flux of 35 kW/m<sup>2</sup>, using an Atlas Cone 2 instrument with a cone shaped heater. Exhaust flow rate was 24 l/s and the spark was continued until the sample ignition. The specimens for cone calorimetry were prepared by the compression molding of the sample (about 30 g) into 3 × 100 × 100 mm square plaques. Typical results from cone calorimetry are reproducible to within  $\pm 10\%$ . The reported results are the average of three determinations. GC–MS data were obtained using an Agilent 6850 series GC connected to an Agilent 5973 Series MS (70 eV electron ionization) with temperature programming from 40 °C to 250 °C. The assignment of peaks utilized co-injection with authentic materials, retention time and analysis of the mass fragmentation patterns.

### 2.3. Preparation of PS, PE and EVA nanocomposites

Polystyrene nanocomposites were prepared by melt blending the polymer with the organically modified clay so that the inorganic content in the nanocomposite was 5% in a Brabender Plasticorder at 190 °C and 60 rpm for 15 min. Synthesis of Zn–Al layered double hydroxide intercalated with 10-undecenoate followed a literature procedure [30], in which zinc

nitrate was substituted for magnesium nitrate. Polyethylene nanocomposites were provided for this study by Frache et al., who prepared a PE–LDH nanocomposite using a zinc–aluminum layered double hydroxide intercalated with stearate anion [4], and Beyer, who reported PE–SWCNT and PE–MWCNT hybrids [6]; all of which were used as-received. The preparation of the terpolymer of styrene, vinylbenzyl chloride and lauryl acrylate, ammonium salt of the terpolymer (here named triclax) and PE–MMT-triclax nanocomposite has been published elsewhere [27].

Modification of LDH–CO<sub>3</sub> with 2-aminotoluene-5-sulfonic acid followed a known procedure [14]. To obtain the EVA–LDH hybrids, the polymer was melt blended with sufficient organically modified clay so that the inorganic content was 3% in a Brabender Plasticorder at 120 ± 5 °C, for 20 min at 60 rpm.

*Nomenclature:* throughout this paper the LDH-undecenoate, the LDH-stearate and the LDH-aminotoluene sulfonate will all be referred to as LDH (even though for polystyrene and polyethylene a Zn–Al LDH was used, a Mg–Al LDH was used for the EVA studies), the MMT-triclax and Cloisite 30B will both be termed as MMT. For the purpose of this study, it is believed that the identity of the nano-dimensional filler material is of greater importance than the specific organic modification used in each case.

## 3. Results and discussion

### 3.1. Morphology of PE nanocomposites

For the PE–LDH nanocomposite, the literature reports XRD patterns that show the complete absence of the typical reflection peaks corresponding to the modified LDH [4] suggesting delamination. From transmission electron microscopy (TEM), the morphology of PE–LDH is best described as mixed intercalated–exfoliated and thus the XRD results must be interpreted as showing disorder of the clay and not complete exfoliation, as had been suggested [4]; the TEM images are shown in Fig. 1. From the low magnification image, one can see that good dispersion of the clay in the polymer has been achieved. The higher magnification image (on

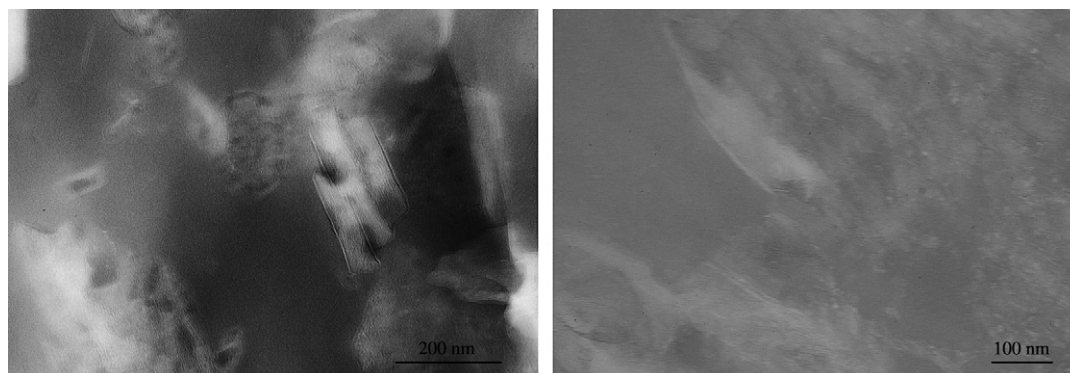


Fig. 1. TEM micrographs of PE–LDH nanocomposite at low and high magnifications (left and right, respectively).

the right) shows the presence of individual clay layers and indicates a mixed intercalated–exfoliated morphology.

Since CNTs do not stack in a periodic fashion, akin to the layered fillers, XRD cannot be used to assess their dispersion in the polymer matrix, thus TEM is the only means for morphological characterization of these systems. Visual inspection of the PE–single-wall nanotube composite is enough to ascertain that the single-wall nanotubes are not well-dispersed in the polyethylene matrix. It is well-known that SWCNT typically appears as ropes or bundles and that there is no good compatibility between the PE polymer matrix and the SWCNT [31], thus it is not a great surprise to observe the lack of good dispersion even on the micrometer level. The results from cone calorimetry also support poor dispersion in this case. The dispersion for PE–MWCNT is good on the micrometer level. From the TEM images (Fig. 2), one can observe large aggregates in the low magnification image along with areas which show only polymer; there is good micro-dispersion but not good nano-dispersion.

The PE–montmorillonite nanocomposite used for this study has also been fully described previously [32]. The XRD trace shows a *d*-spacing of 3.7 nm which is the same value as seen in the virgin organo-clay. The TEM shows good dispersion in the low and high magnification images, indicating that polymer intercalation has probably occurred. From cone calorimetry the reduction in the peak heat release rate is 70%, which is another indication of good nano-dispersion of the clay in the PE matrix.

### 3.2. Thermal degradation of PE nanocomposites

The thermal degradation of the three nano-dimensional filler materials used in this study was accessed using thermogravimetric analysis (TGA) and the TGA curves for all the three are shown in Fig. 3. It is obvious that the carbon nanotubes show excellent thermal stability and no mass loss is seen, while the organically modified LDH is the least stable of these three materials. The oligomerically modified MMT used is particularly stable for an ammonium bearing clay [27,33], and this is also obvious from the figure. It should also be noted that the oligomerically modified clay contains

a relatively high molecular weight surfactant so the inorganic content of the clay is low, as is obvious from the figure.

The TGA curves for the PE nanocomposites are shown in Figs. 4 and 5 and the characteristic degradation temperatures are summarized in Table 1. As expected, the poor dispersion of SWCNT led to no change in both the onset temperature,

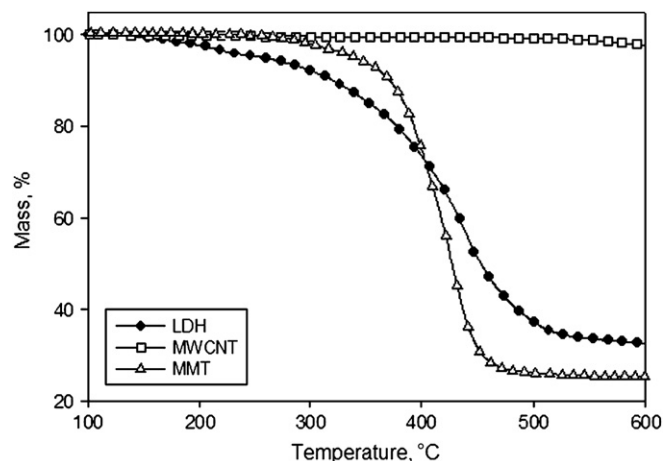


Fig. 3. TGA curves of LDH, MWCNT and MMT.

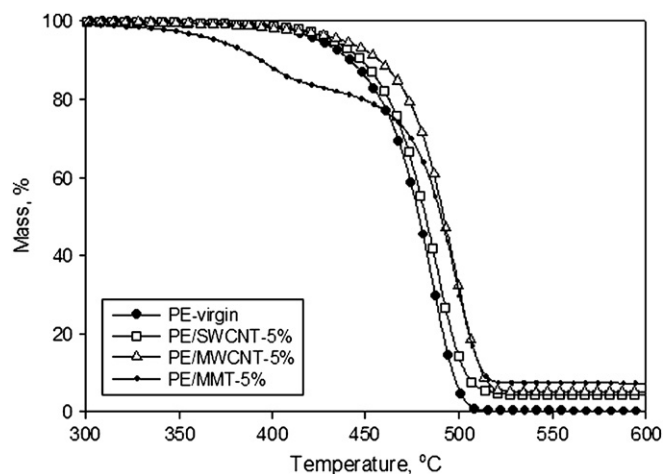


Fig. 4. TGA curves of PE and its nanocomposites.

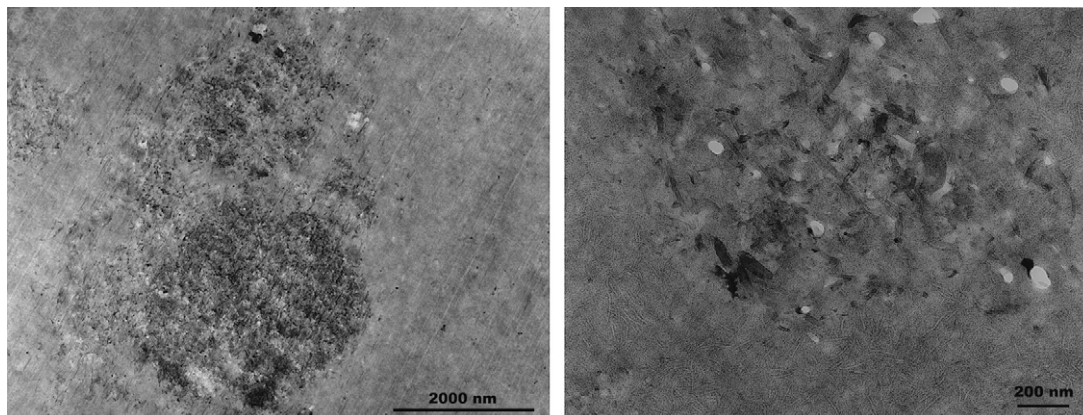


Fig. 2. TEM micrographs of PE–MWCNT nanocomposite at low and high magnifications (left and right, respectively).

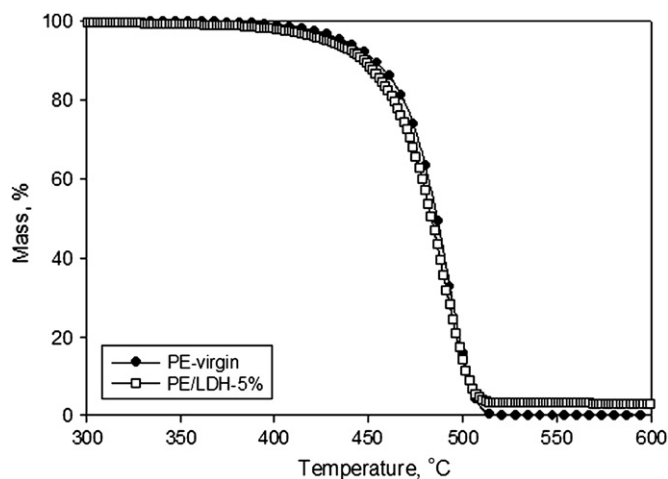


Fig. 5. TGA curves of PE and its LDH nanocomposite.

Table 1  
Summary of TGA results for PE and its nanocomposites

Sample	$T_{0.1}$ (°C)	$T_{0.5}$ (°C)	$\Delta T_{0.5}$ (°C)
PE	441	478	—
PE–SWCNT	446	481	3
PE–MWCNT	457	491	13
PE–LDH	439	475	–3
PE–MMT	393	490	12

$T_{0.1}$  = temperature at 10% mass loss;  $T_{0.5}$  = temperature at 50% mass loss;  $\Delta T_{0.5}$  = temperature difference at 50% mass loss between the nanocomposite and the virgin PE.

herein defined as the temperature at which 10% degradation occurs,  $T_{0.1}$ , and the temperature at which 50% degradation occurs,  $T_{0.5}$ . For both MMT and MWCNT, the temperature at which 50% mass loss occurs increases by about 13 °C, indicating similar thermal stability for these two. The oligomeric surfactant used for the modification of MMT is likely responsible for the initial destabilization of the nanocomposite, given the amount which it is present (about 20% out of the total PE–MMT composition) and its onset degradation temperature (*cf.* Fig. 3). The LDH did not bring about a similar enhancement, most likely due to its inherent lower thermal stability (*cf.* Fig. 3).

One of the most important parameters for evaluating the flammability properties by cone calorimetry is the reduction in the peak heat release rate (PHRR), which gives a measure of the size of the fire. The results for PE nanocomposites [4,6] are summarized in Table 2. The largest reduction in the PHRR is seen for the two clays, followed by a lower reduction for the multi-wall nanotubes and no reduction (in fact, an apparent increase) for the single-wall nanotubes. The difference between the two nanotube composites is easily explained by the dispersion for each; poor dispersion at the micrometer level for the SWCNT and good micrometer dispersion but relatively poor nano-dispersion for the MWNT. Both of the clays, MMT and LDH, show good dispersion at the nanometer level and the reduction in the PHRR is similar for both. This point will be revisited later in this paper.

Table 2

Cone calorimetric results of PE and its nanocomposites (heat flux is 35 kW/m<sup>2</sup>)

Sample	PE	PE–SWCNT	PE–MWCNT	PE–LDH	PE–MMT
PHRR reduction (%)	—	–50	35	55	60

The usual explanation for the reduction in the peak heat release rate is that this is due to concomitant changes in the mass loss rate. The reduction in the mass loss rate is ascribed to the formation of a barrier which prevents mass transfer and thermally insulates the underlying polymer from the heat source [10]. This barrier has been usually thought of as arising from erosion of the polymer, exposing the clay; recently an alternative explanation, which suggests that the surface energy of the clay is enough that it will rise to the surface at temperatures well below those at which thermal degradation of the polymer occurs, has been proposed [34]. It has been very recently suggested that the formation of the barrier actually occurs after the clay has made its presence known through a process that has been called nano-confinement [35]. Nano-confinement means that the clay platelets function as a barrier within the polymer matrix and keep the degrading polymer radicals together for some time.

In a series of papers from these laboratories, it has been shown that the products of thermal degradation of nanocomposites are different from those of the virgin polymers when the reduction in the peak heat release rate is large, and that there is no change in thermal degradation products for those systems which show a modest change in the PHRR. The interpretation of this is that the degrading polymer radicals are momentarily trapped by the clay platelets for long enough time to permit radical recombination reactions, which reform a polymer so that the degradation will occur over a longer time period with a reduced peak heat release rate. The changes have been correlated with the stabilization energy of the radicals formed in the degradation; when the radicals have a high stabilization energy, they have a sufficient life time to permit these recombination reactions, *e.g.*, the styryl radical from polystyrene and the allylic radical from EVA. For a radical without a high stabilization energy, such as a radical adjacent to a nitrile from SAN, the reactions do not occur and a much smaller reduction in the PHRR is observed [11–16].

In order to better understand these systems, TGA/FTIR studies of the thermal degradation were carried out. There were no marked differences in the infrared spectra when the virgin polymer was compared to composites reinforced with either the MMT, LDH, MWCNT or the SWCNT. Thus, the evolved degradation products were collected using a cold trap and then analyzed by GC–MS. The GC trace for virgin polyethylene shows a series of three peaks from about C<sub>9</sub> to C<sub>31</sub>, corresponding to the  $\alpha,\omega$ -diene, terminal alkene and alkane. The GC traces between C<sub>21</sub> and C<sub>23</sub> for virgin polyethylene and the composites with LDH, MMT, MWCNT and SWCNT are shown in Fig. 6.

In the case of PE–MMT, a dramatic change in terms of evolved products occurs compared to virgin PE. The diene

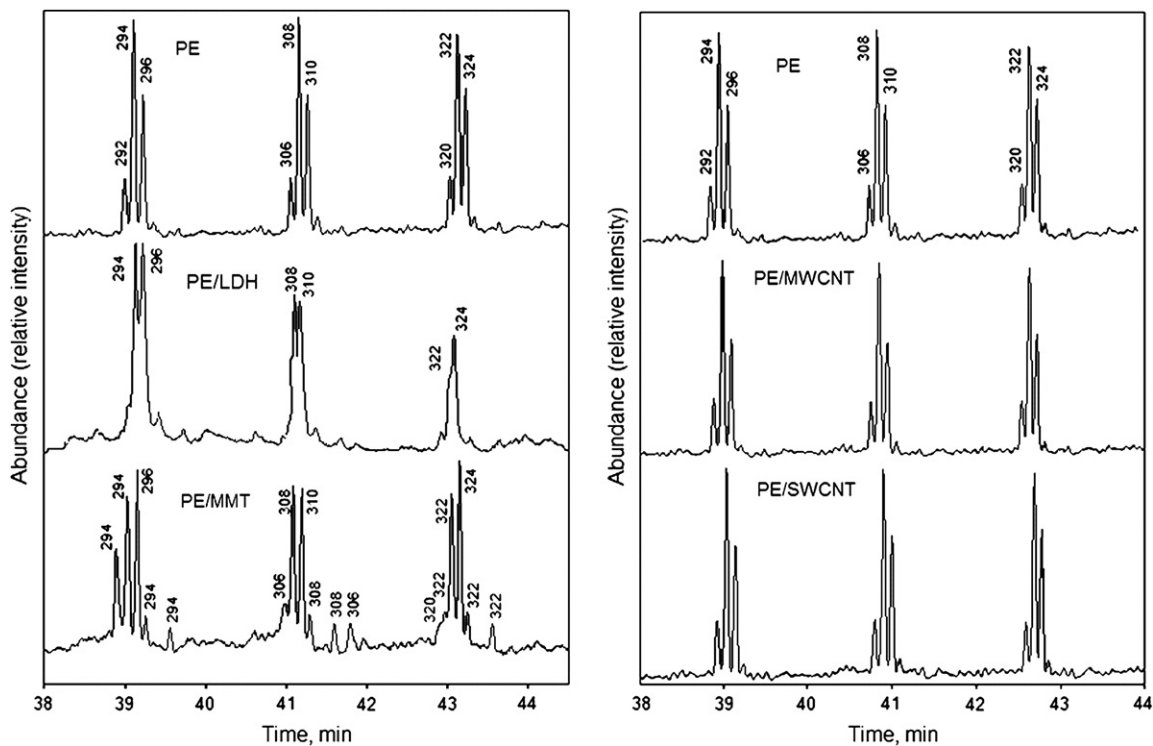


Fig. 6. Selected GC–MS chromatograms ( $C_{21}$ – $C_{23}$  region) of the PE and its nanocomposites.

peaks are very much reduced and a series of internal olefins are produced in small amounts. In addition, the alkane peaks are visibly increased, becoming the strongest, and the signal to noise ratio seems to decrease due to the presence of numerous noise-like peaks, which may indicate the formation of new compounds. These changes are in excellent agreement with what has been previously observed for PE–MMT nanocomposites [16]. For the LDH, one also sees a change in the composition of the volatiles, the  $\alpha,\omega$ -diene seems to vanish and the amounts of the alkene and alkane are now comparable; the changes in the degradation pathway are similar for MMT and LDH based composites. In contrast, both single-wall and multi-wall nanotube composites show identical products to those produced from unfilled polyethylene; there is no change in product ratio and no additional products are observed.

The thermal degradation of polyethylene is initiated by random scission followed by hydrogen abstraction to give a new radical site. Since the products are the same as those from the degradation of ethylene–vinyl acetate copolymer (EVA), which degrades initially by chain stripping to lose acetic acid and form poly(ethylene-*co*-acetylene), double bonds must be produced during the degradation process which leads to the formation of an allylic radical which has sufficient stabilization energy to undergo radical recombination reactions. A generalized scheme has been previously reported for the degradation of polyethylene [36].

The tentative conclusion from this portion of this study is that both MMT and LDH based composites give changed degradation products, while no change is noted for the PE–carbon nanotube composites. These points will be revisited after the

results for the other systems, ethylene–vinyl acetate copolymer (EVA) and polystyrene, are described.

### 3.3. Morphology of EVA/clay hybrids

When the LDH-carbonate (LDH- $CO_3$ ) was anion exchanged with aminotoluene sulfonate, the *d*-spacing increased from 0.78 nm to 1.67 nm. However, upon melt blending with EVA, no further expansion of the intergallery space was observed (see Fig. 7), suggesting a microcomposite morphology. This finding is interesting because for EVA–Cloisite

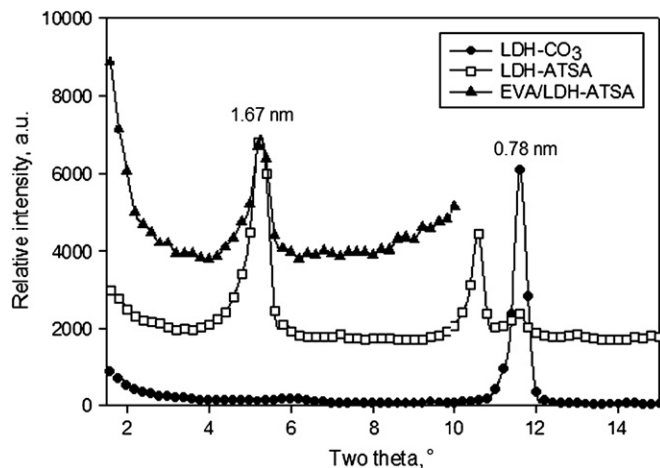


Fig. 7. XRD patterns of LDH-carbonate, organically modified LDH and EVA/LDH hybrid.

30B with a  $d$ -spacing only 0.2 nm larger (1.85 nm) allowed the formation of a delaminated nanocomposites [13]. The TEM micrographs presented in Fig. 8 show relatively good microdispersion of LDH in EVA with tactoids of about 200–300 nm in diameter, but no clear sign of delamination or intercalation.

The TEM images of MWCNT in EVA are shown in Fig. 9; the low magnification image shows rather good dispersion, with only few areas in which one can observe aggregation of nanotubes. From the high magnification image, the diameter of the CNT can be estimated as 5–15 nm. The overall dispersion of MWCNTs is significantly better for EVA than that observed for PE, which is, perhaps, not surprising considering that PE is non-polar while EVA has some polarity due to the presence of the acetate.

#### 3.4. Thermal degradation of EVA nanocomposites

The TGA curves of EVA and its nanocomposites show two degradation steps: the loss of the acetic acid and the main degradation step (see Fig. 10). The presence of LDH or MWCNT does not bring about any acceleration of the acetic acid loss, as has been observed with MMT [13]; the explanation that has been offered for this acceleration in the case of

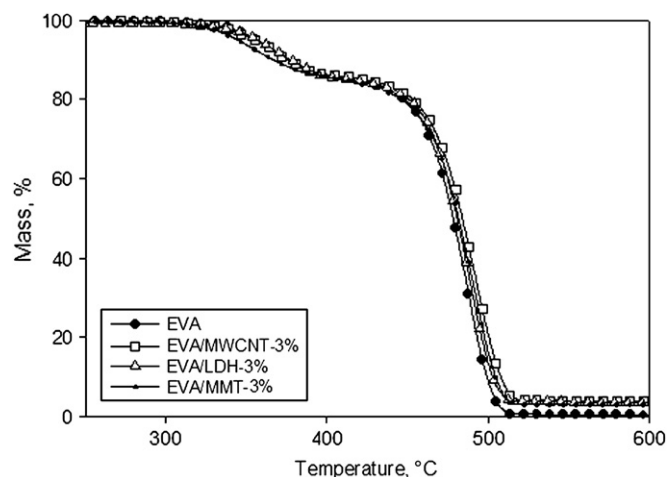


Fig. 10. TGA curves of EVA and its nanocomposites.

MMT is the presence of acidic sites which are thought to catalyze the deacetylation reaction [37]. This step is magnified in Fig. 11 so that it may be clearly seen. In the main degradation region, for all the three systems, one can see a slight stabilization that is typical for EVA nanocomposites [13] (Fig. 12).

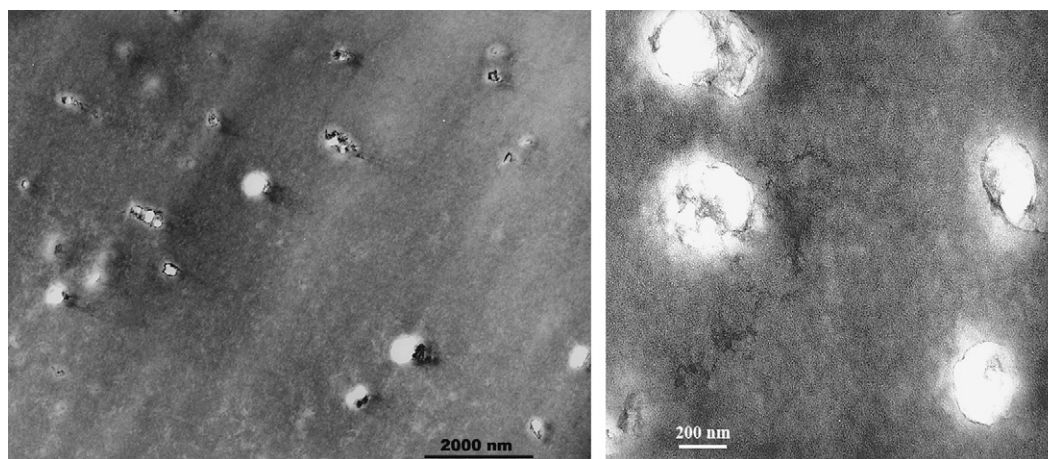


Fig. 8. TEM micrograph of EVA/LDH nanocomposite at low and high magnifications (left and right, respectively).

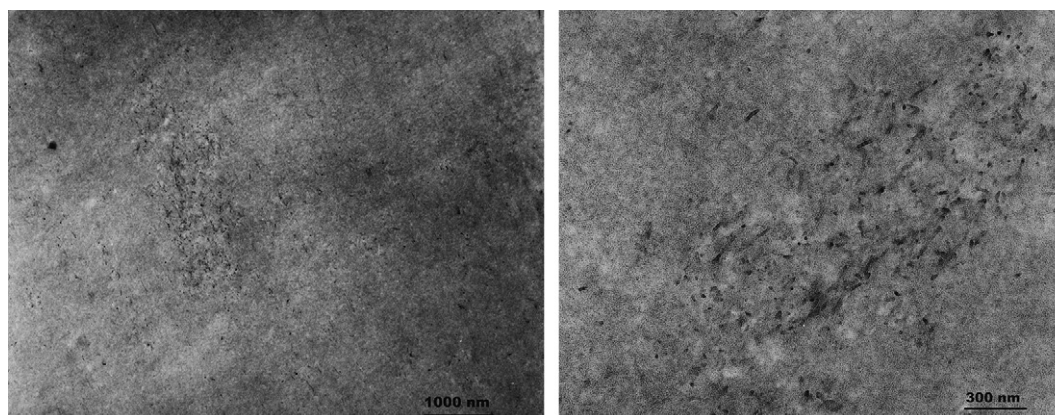


Fig. 9. TEM micrographs of EVA/MWCNT nanocomposite at low and high magnifications (left and right, respectively).

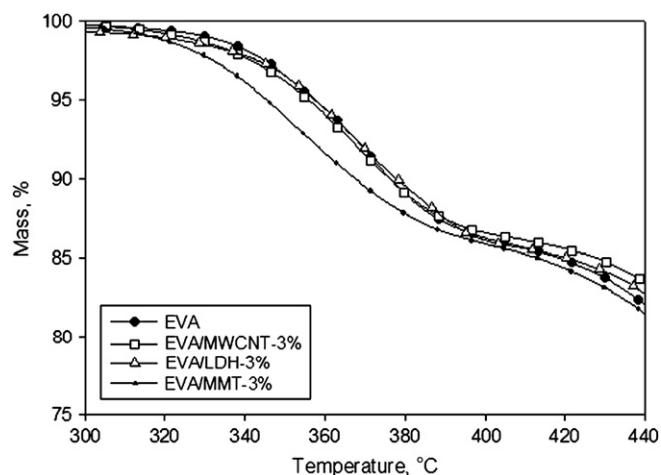


Fig. 11. TGA curves of EVA and its nanocomposites (expansion of the first degradation step).

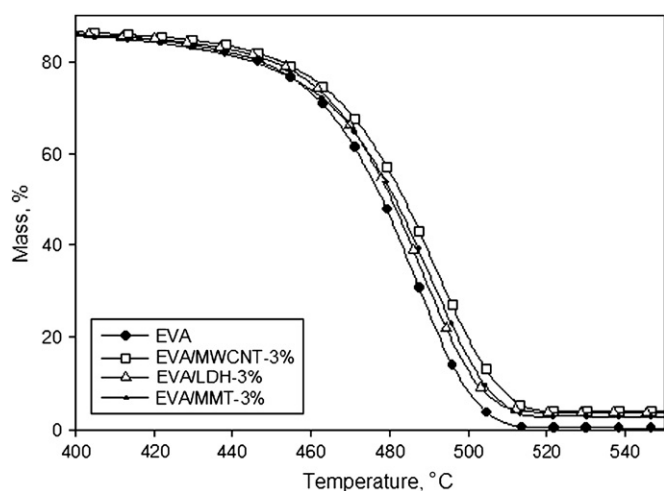


Fig. 12. TGA curves of EVA and its nanocomposites (expansion of the second degradation step).

The cone calorimetric results (summarized in Table 3) show significant PHRR reductions for all nanocomposites, while the total heat release stays the same, indicating that all of the polymers will eventually burn. MWCNT gives a significantly larger reduction in PHRR than does MMT, which may be explained by consideration of the appearance of the char left behind upon burning of the two nanocomposites and the burning times, as seen in Fig. 13. In the case of CNT, the char is very compact and strong, while for MMT it is more fragile and cracked and thus less effective in reducing mass/

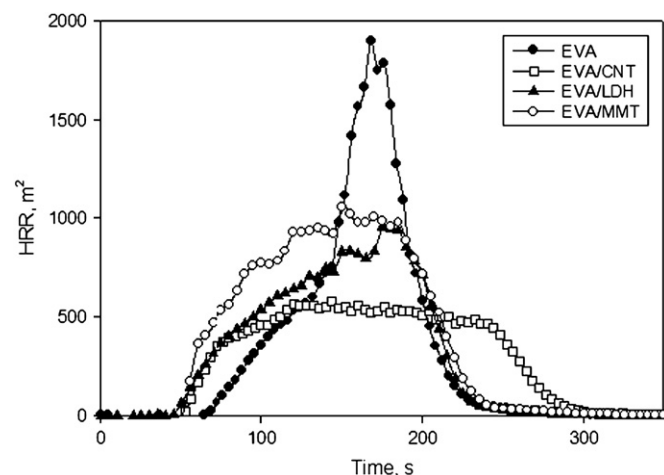


Fig. 13. HRR plots for EVA and its nanocomposites (at a heat flux of  $35 \text{ kW/m}^2$ ).

heat transfer. The larger size of the CNT may also play a role in the char strength and ability to retain flammable degradation products, which translates into a prolonged burning time. One usually expects the morphology of the composite to have an effect on the reduction in the peak heat release rate; an intercalated or delaminated morphology will give the maximum reduction in PHRR, while one in which there is some immiscible (microcomposite) phase will give a lower reduction. Both the CNT and the MMT systems show good nano-dispersion and give large reductions in the PHRR, while the LDH shows relatively poor nano-dispersion and a lower, but still quite significant, reduction in the PHRR.

The degradation products (collected as described above) were analyzed using GC–MS. As it can be seen in Fig. 14, there is no marked difference between virgin EVA and its MWCNT and LDH nanocomposites. In contrast, the presence of MMT in the polymer matrix leads, just as in the case of PE, to the formation of an increased amount of saturated species and a small amount of internal olefins. The changes observed in the vapor phase must be related to those in the condensed phase, since this is the only available hydrogen source, thus suggesting that hydrogen abstraction or other reactions occur, leading to transient crosslinking. Based on the work on the PE systems, one might claim that the poorer dispersion of the LDH in EVA leads to no change in degradation products, while for PE better dispersion resulted in a change in the degradation process. A tentative conclusion then is that the degradation pathway may be changed when the clay is well-dispersed at the nanometer level, but there is no change if this level of dispersion is not achieved. Similar results have

Table 3

Cone calorimetric results for EVA and its nanocomposites (heat flux of  $35 \text{ kW/m}^2$ )

Composition	PHRR ( $\text{kW/m}^2$ )	Reduction (%)	THR ( $\text{MJ/m}^2$ )	ASEA ( $\text{m}^2/\text{kg}$ )	AMLR ( $\text{g/s m}^2$ )	$t_{ig}$ (s)
EVA	$1772 \pm 170$	—	$112 \pm 4$	$399 \pm 7$	$23.5 \pm 0.3$	$75 \pm 3.6$
EVA/CNT (3%)	$597 \pm 30$	66	$101 \pm 1$	$553 \pm 37$	$13.9 \pm 0.6$	$63 \pm 1.1$
EVA/LDH (3%)	$1090 \pm 58$	39	$106 \pm 3$	$468 \pm 23$	$18.0 \pm 0.3$	$57 \pm 1.2$
EVA/MMT (3%)	$903 \pm 24$	49	$99 \pm 4$	$515 \pm 43$	$14.6 \pm 0.7$	$60 \pm 2.1$

PHRR, peak heat release rate; THR, total heat release; ASEA, average specific extinction area, a measure of smoke; AMLR, average mass loss rate;  $t_{ig}$ , time to ignition.

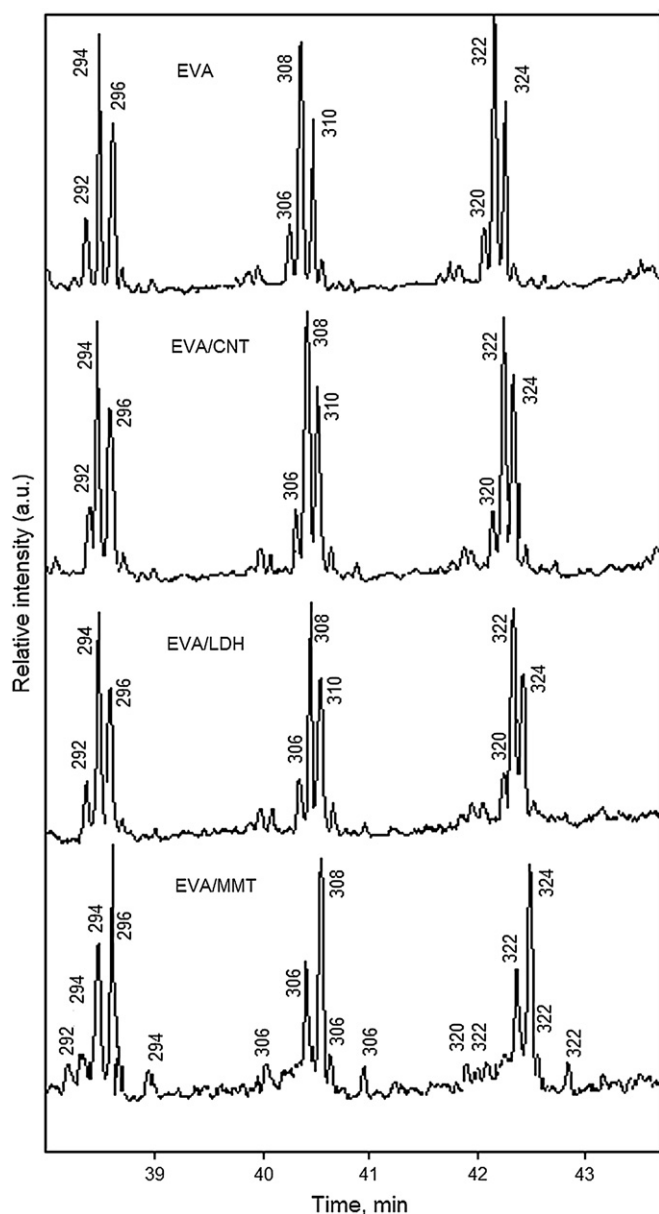


Fig. 14. Selected GC–MS chromatograms ( $C_{21}$ – $C_{23}$  region) of the EVA and its nanocomposites.

already been observed with MMT in EVA; when an organically modified clay is well-dispersed in EVA there is a change in degradation pathway and an associated large reduction in PHRR, whereas when an inorganic clay is used, which is not well-dispersed, there is no change in PHRR or the degradation pathway. On the other hand, for CNT there can be a large reduction in the PHRR for both well-dispersed and less well-dispersed systems, which suggests that a different mechanism is operative for CNT than for the clays.

### 3.5. Morphology of PS nanocomposites

The XRD traces of PS–MMT (Fig. 15) show an increase in the  $d$ -spacing of 0.5 nm as compared to the modified clay, suggesting the typical intercalated structure for these

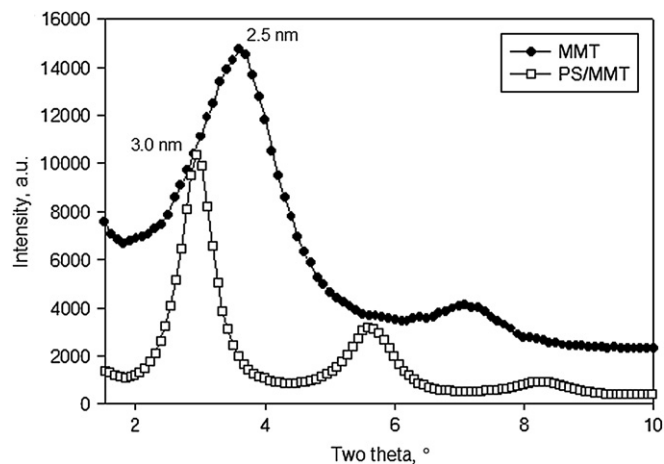


Fig. 15. XRD patterns of MMT and PS–MMT.

systems [28,38,39]. The TEM micrographs, presented in Fig. 16, show the presence of relatively large, but well-dispersed, clay tactoids in the polymer matrix; in the high magnification image, one can clearly see the expanded clay layer, which is indicative of an intercalated morphology, supporting the XRD observations.

In the case of PS–LDH, the low magnification TEM micrograph shows good dispersion of LDH in PS at the microscale, but not at the nanoscale (Fig. 17). The lack of any increase in the  $d$ -spacing in the XRD pattern, as seen in Fig. 18, and the absence of any indication of intercalation or exfoliation from the high magnification TEM images (not shown here) suggest the formation of an immiscible nanocomposite (microcomposite).

The dispersion of CNT in PS is very good. In the low magnification TEM micrographs (Fig. 19) one can see very little agglomeration of nanotubes, which are uniformly distributed throughout the polymer matrix; the high magnification image shows individual, unbundled, nanotubes, with a diameter of 15–20 nm.

### 3.6. Thermal degradation of PS nanocomposites

From the TGA curves in Fig. 20, it is apparent that the addition of CNT and MMT enhances the thermal stability of PS (both in terms of the onset of degradation and the mid-point temperature,  $T_{0.1}$  and  $T_{0.5}$ , respectively), but the lower thermal stability of LDH and its poorer dispersion lead to smaller improvements (Table 4).

The cone calorimetric results for the PS nanocomposites are shown in Fig. 21 and are summarized in Table 5 and show very good reductions for the two well-dispersed nanomaterials (MMT and CNT). Also, since the PHRR reductions are the same (58% and 60%, respectively) and the two HRR curves basically superimpose, it is tempting to assume that whatever mechanism is responsible for the PHRR reduction in one case will be the same for the other (an assumption that is proven wrong by the analysis of the corresponding degradation products for the two nanocomposites, *cf.* next). The

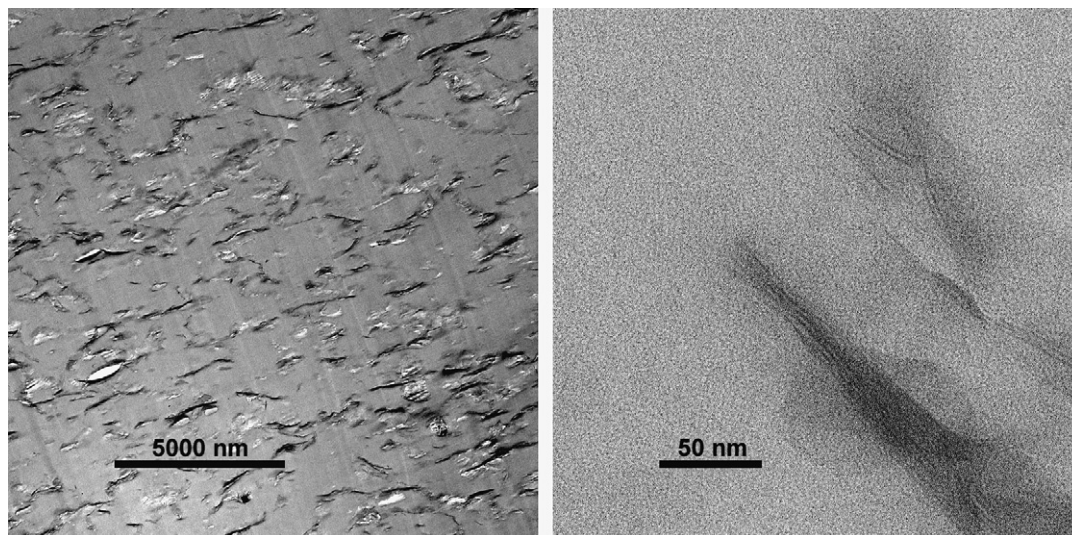


Fig. 16. TEM micrographs of PS–MMT nanocomposite at low and high magnifications (left and right, respectively).

other nanomaterial, LDH, even though not perfectly dispersed at the nanometer level, gave a fairly good PHRR reduction of 35% for a microcomposite; for comparison, for poorly dispersed MMT one expects essentially no reduction in the peak heat release rate for a PS–MMT microcomposite [40].

When the degradation products were collected and analyzed by GC–MS, the virgin PS evolved mainly monomer, dimer and trimer, as expected (Fig. 22). The presence of MMT leads to the formation of a series of recombination products, as reported before [11]. However, when CNT fillers are added there seems to be no effect on the degradation products of PS, as seen from the almost identical chromatograms of the PS and PS–CNT. Thus CNTs do not have the same effect on PS degradation as MMT – as might have been expected, given the similar morphology and the almost identical cone calorimetric

behavior as with PS–MMT. This observation is in very good agreement with the behavior seen here for the PE and EVA systems. The LDH does not change the degradation products of PS, as also was seen with EVA but not with PE.

Based on the observations made on polymer–MMT systems, it was initially hypothesized that the presence of the filler acting as barrier leads to a longer residence life for the degrading radicals (nano-confinement is another expression of this phenomenon), which can in turn lead to recombination products, providing that the radicals have high enough stabilization energy. The chemical identity of the barrier was thought to be of little importance, as long as it provided enough time for the recombination reactions to take place. In order to explain how MMT interacts with the degrading radicals, two theories have been formulated.

Firstly, the paramagnetic iron present in MMT, either as impurity or as structural iron, was shown to play a role in radical trapping and account for the PHRR reduction at low clay loadings [41]. Thus, one may envision the iron mediating the observed radical recombination reactions.

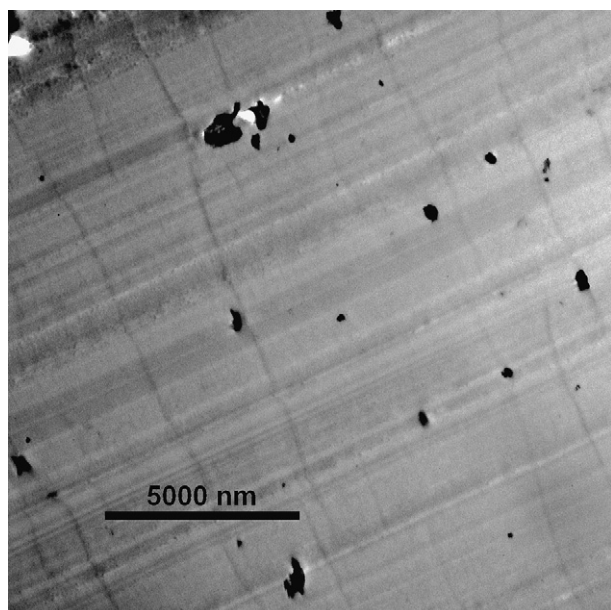


Fig. 17. TEM micrographs of PS–LDH nanocomposite at low magnification.

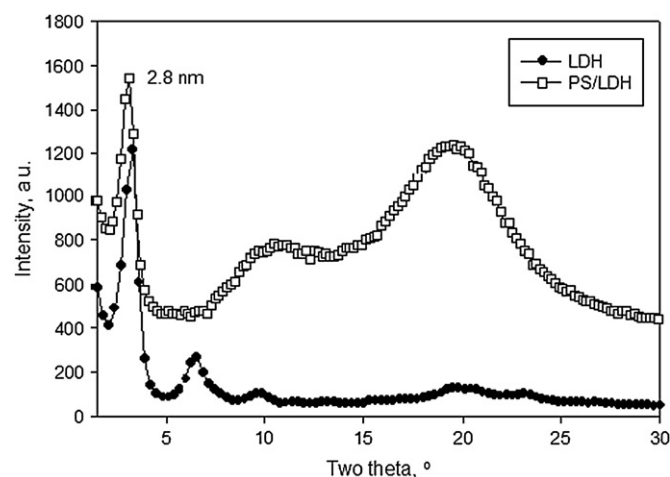


Fig. 18. XRD patterns of LDH and PS–LDH.

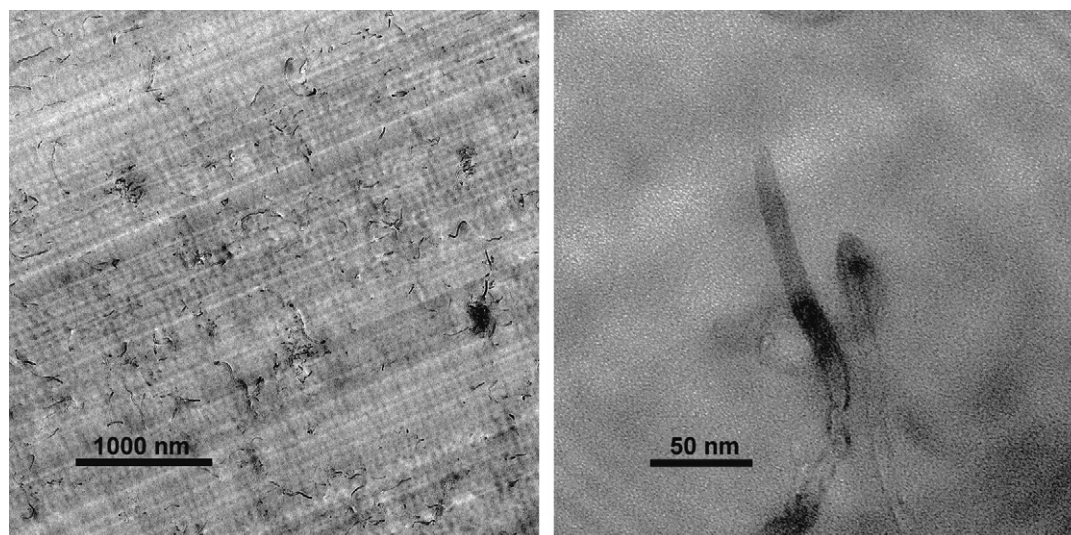


Fig. 19. TEM micrographs of PS–CNT nanocomposite at low and high magnifications (left and right, respectively).

Secondly, the proposed catalytic action of the montmorillonite on the degrading radicals may be related to the presence of the edge hydroxyl groups on the perimeter of the clay. Therefore, if the catalytic effect involves these hydroxyls, they can be replaced to examine the effect on the degradation products of PS. A third possible hypothesis, which has not been tested, is that acid sites on the surface, not the edge, are involved in catalysis.

To test the two hypotheses, two additional PS nanocomposites were prepared, under similar conditions as above, one

with iron-free MMT clay (acquired from Source Clay) and a second in which the edge hydroxyl groups were reacted with chlorotrimethylsilane [42]. The degradation products from both the samples were collected and analyzed by GC–MS. As seen from the chromatograms shown in Fig. 23, as well as from their expansion of the dimer region (Fig. 24), there is no difference between the PS–MMT (iron-containing clay) and the PS–iron-free MMT, suggesting that iron is not responsible for the changes in the degradation pathway. Moreover, PS–MMT–TMS (OH-free MMT sample) gave the same results as the standard MMT sample, suggesting that as far as the degradation products are concerned, the presence or absence of the edge hydroxyls does not make a difference either.

### 3.7. Mechanism of action for MMT, LDH and carbon nanotubes

The current explanation for the reduction in the peak heat release rate, *i.e.*, the fire retardancy, of montmorillonite-based

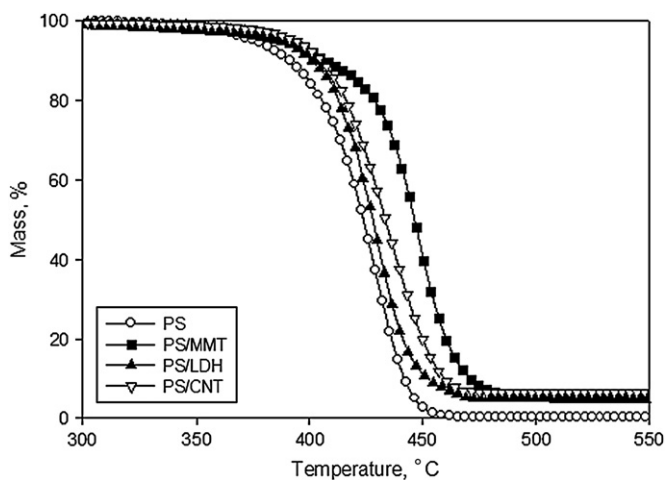


Fig. 20. TGA curves for PS and its nanocomposites.

Table 4  
TGA results for PS and its nanocomposites

Sample	$T_{0.1}$ (°C)	$T_{0.5}$ (°C)	$\Delta T_{0.5}$ (°C)
PS	390	424	NA
PS–CNT	404	433	9
PS–LDH	399	428	4
PS–MMT	412	445	21

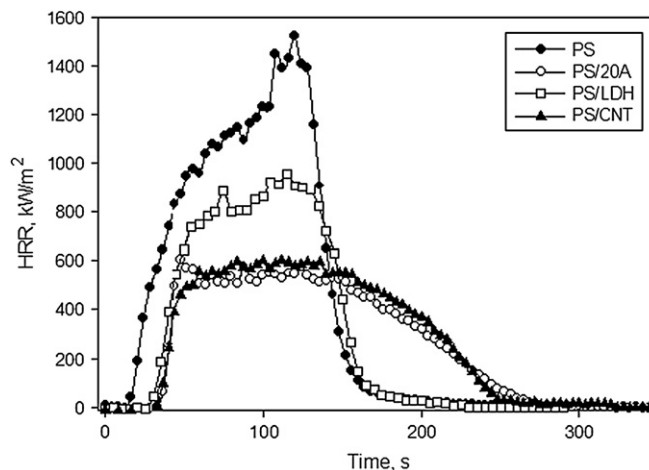


Fig. 21. HRR curves for PS and its nanocomposites.

Table 5  
Summary of the cone calorimetric results for PS and its nanocomposites

Sample	PHRR (kJ/m <sup>2</sup> )	Reduction (%)	THR (MJ/m <sup>2</sup> )	ASEA (m <sup>2</sup> /kg)	AMLR (g/s m <sup>2</sup> )	<i>t</i> <sub>ig</sub> (s)
PS	1475 ± 37	NA	94 ± 3	1338 ± 36	31 ± 1	54 ± 1
PS–MMT	592 ± 43	60	90 ± 1	1520 ± 28	15 ± 0	46 ± 1
PS–CNT	620 ± 5	58	96 ± 1	1369 ± 34	16 ± 0	43 ± 1
PS–LDH	956 ± 24	35	94 ± 1	1382 ± 14	25 ± 1	41 ± 1

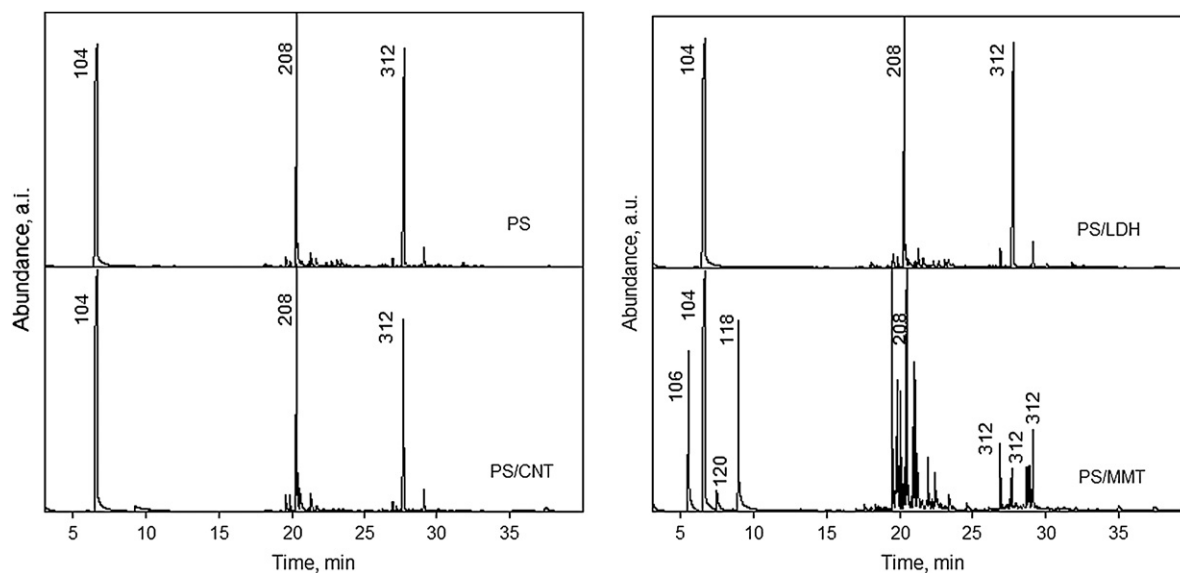


Fig. 22. GC–MS chromatograms for PS and its nanocomposites.

nanocomposites is that a barrier is formed which inhibits mass transfer and provides thermal insulation to shield the underlying polymer from the fire source. Kashiwagi et al. have examined a number of carbon nanotube-based nanocomposites and suggest that (a) the dispersion of the nanotubes is of critical importance and that (b) only a very small loading, typically less than 1%, is sufficient to give a significant reduction in the PHRR. Carbon nanotubes give a denser barrier than that is typically obtained with MMT [7–9]. In the case of LDH, it has been stated that as, *e.g.*, with epoxy-LDH nanocomposites, a compact intumescent residue is formed, which also has good mechanical strength [8]. The process in all nanofiller cases appears to be barrier formation with a variation depending upon the strength of the barrier.

When this work commenced, the hope was that one would be able to tell if the barrier formed — and which results in the significant reductions in the peak heat release rate of nanocomposites compared to virgin polymers — is physical or chemical in origin. If only a physical barrier is produced, then the identity of the barrier should be unimportant and any nano-dimensional filler material should give a similar reduction in the PHRR and show the same changes in product composition. On the other hand, if a chemical barrier is formed, *i.e.*, if there is some chemical interaction between the degrading radicals and the nano-dimensional filler material, then one should see variations in both the PHRR and the compositions of the products.

A comparative discussion of the results presented here shows that there is a similar reduction in the peak heat release rate for PE–LDH and PE–MMT and a smaller decrease for PE–CNT composites. The CNT system shows good microdispersion but not nano-dispersion while there is better nano-dispersion for both the MMT and the LDH systems. In this case, it seems that the type of filler dispersion in the PE is the significant difference; good nano-dispersion, as seen with MMT and LDH, gives a large reduction in the PHRR while poorer nano-dispersion, as seen for CNT, results in a lower reduction. In addition, a change in the degradation pathway of PE — as manifested by the thermal degradation products — in the presence of both MMT and LDH but not with CNT suggests that dispersion is one critical issue in achieving significantly enhanced fire performance. The observation of a measurable reduction in the PHRR, albeit poor dispersion at the nanometer level, for CNT-filled PE suggests that a different mechanism is operative for this nano-dimensional filler material.

For EVA, the largest reduction in PHRR is achieved for CNT, with a smaller reduction for MMT, even though both are well-dispersed. The LDH shows the poorest dispersion and the lowest reduction in PHRR, which is likely directly related to the lack of a change in the degradation process. It is possible that well-dispersed CNT is inherently more efficient than MMT in reducing the PHRR.

The results for polystyrene are quite similar to those with EVA. Both MMT and CNT show good dispersion and similar

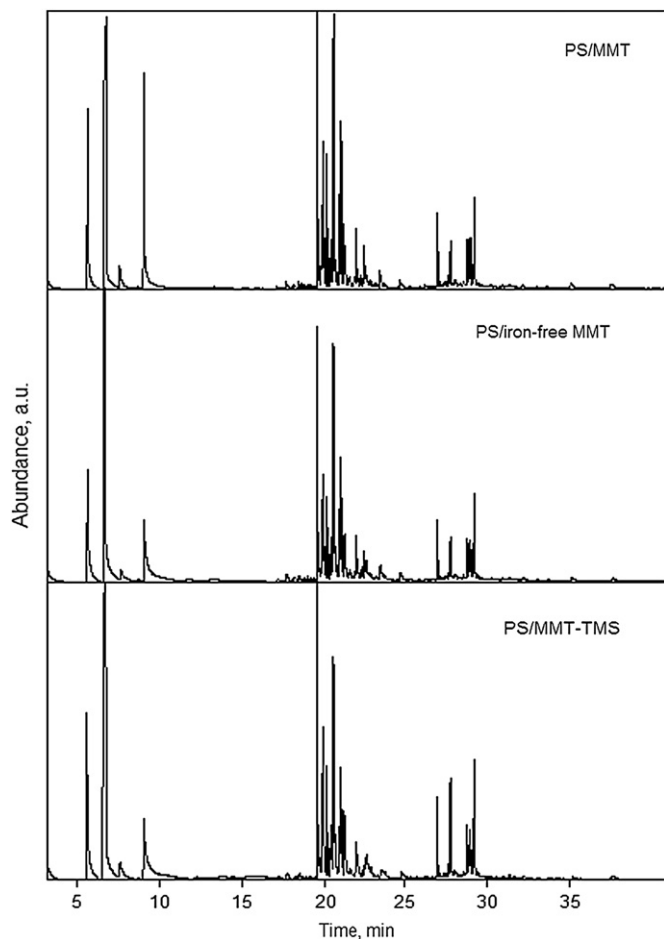


Fig. 23. GC–MS chromatograms for PS nanocomposites with iron-free, iron-containing and OH-free MMT.

reductions in PHRR, while LDH is not as well-dispersed and shows a lower reduction.

We currently feel that for all the three nanomaterials, the quality of dispersion is of paramount importance; a well-dispersed nanomaterial will give a large reduction in the PHRR. When an LDH is well-dispersed at the nanometer level, the reduction in PHRR and the change in degradation pathway are quite similar to that for well-dispersed MMT. On the other hand, for CNT there is no change in the degradation pathway of the polymer, independent of dispersion at the nanometer level. However, the reduction in the PHRR is much larger than would be expected for poorly dispersed MMT (microcomposite). This suggests that the reduction in flammability that is observed for CNT composites and nanocomposites should be attributed to a process which is different from the one which is operational for MMT and LDH.

When the LDH is well-dispersed at the nanometer level, the reduction in PHRR and the degradation pathway is similar to that of MMT. However, even with relatively poor dispersion, LDH can have a strong reduction in the PHRR. This is in contrast with MMT layered silicates, for which usually a microcomposite, *i.e.*, a system with poor filler dispersion, will give a very low, essentially no, reduction in PHRR while a nanocomposite, whether intercalated or delaminated, will

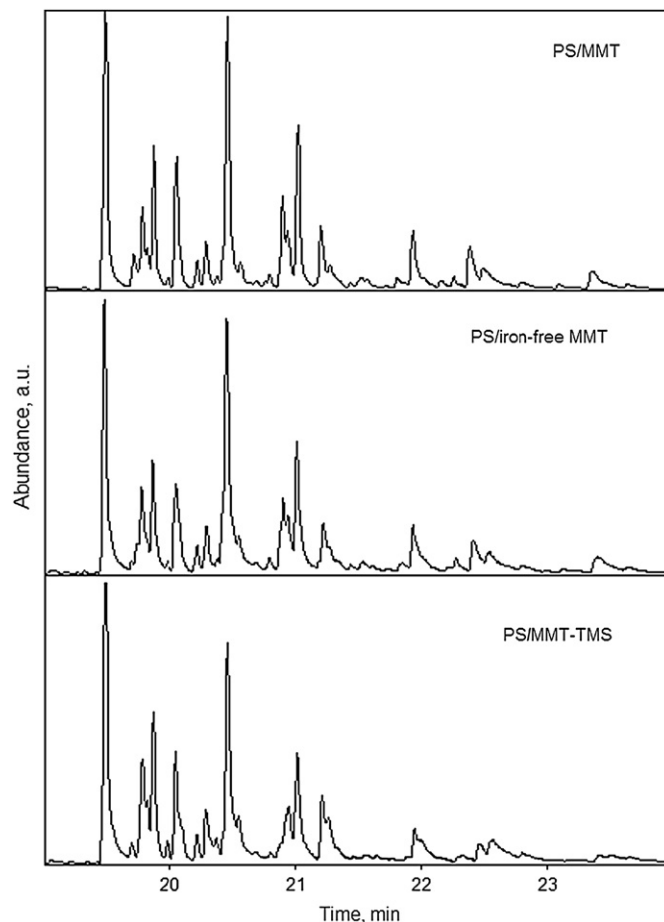


Fig. 24. GC–MS chromatograms for PS nanocomposites with iron-free, iron-containing and OH-free MMT (expansion of the dimmer region).

give substantial reduction. One may suggest that there is some similarity between the mechanism of action of silica and LDH. Silica, with a large number of hydroxyl groups attached, can hydrogen bond at higher temperatures to form a barrier and this can prevent volatilization of the polymer [43–45]. A similar process may occur with the LDH, by producing a large surface area mass which acts as a barrier to heat and mass transport. One may also wish to consider that an LDH will eliminate water at 400–500 °C and this water will dilute the combustible gases, which may exert a fire retardant effect. One may further speculate that if an LDH which is not well-dispersed gives this result, will a well-dispersed material not be better?

#### 4. Conclusions

Polyethylene, ethylene–vinyl acetate copolymer and polystyrene nanocomposites were prepared using montmorillonite, layered double hydroxides and carbon nanotubes as the nano-dimensional filler material. In each case, there is a substantial reduction in the peak heat release rate but only for PE–MMT, PE–LDH, EVA–MMT and PS–MMT the products of thermal degradation changed by the nanocomposite formation. The composite morphologies, as accessed by XRD and TEM, differ for the various nanocomposites, and these morphological

differences may be one reason for the differences in thermal degradation of these nanocomposites. The morphologies for the EVA and PS systems are fairly similar, with at least MMT and the carbon nanotube showing good nano-dispersion, yet even with this system, there are ambiguities. While MMT clearly changes the degradation products in all polymers studied, addition of LDH or CNT does not have the same effect. Finally, the presence of iron in MMT and of edge hydroxyls on MMT was evaluated by using models – iron-free and edge-silicated MMTs – and neither of these two parameters seems to be responsible for its FR behavior. This investigation, despite the insights it provides, does not fully answer the question about a physical vs. a chemical barrier mechanism as the reason for the reduction in the peak heat release rate, and further work is necessary to address this question.

### Acknowledgements

We gratefully acknowledge conversations with Alexander Morgan which have been very useful in formulating the ideas herein presented. M.J.H. and E.M. acknowledge support through an ES&F fellowship by the Penn State ARL.

### References

- [1] Alexandre M, Dubois P. *Mater Sci Eng* 2000;R28(1):1–63.
- [2] Okada A, Usuki A. *Mater Sci Eng* 1995;C3:109.
- [3] Zhu J, Morgan AB, Lamelas FJ, Wilkie CA. *Chem Mater* 2001;13:3774–80.
- [4] Ray SS, Okamoto M. *Prog Polym Sci* 2003;28:1539–641.
- [5] Utracki LA, Sephr M, Boccaleri E. *Polym Adv Technol* 2007;18:1–37.
- [6] Okada A, Usuki A. *Macromol Mater Eng* 2007;291:1449–76.
- [7] Costantino U, Gallipoli A, Nocchetti M, Camino G, Bellucci F, Frache A. *Polym Degrad Stab* 2005;90:586–90.
- [8] Zammarano M, Franceschi M, Bellayer S, Gilman JW, Meriani S. *Polymer* 2005;46:9314–28.
- [9] Beyer G. *Fire Mater* 2005;29:61–9.
- [10] Kashiwagi T, Du F, Douglas JF, Winey KI, Harris Jr RH, Shields JR. *Nat Mater* 2005;4:928–33.
- [11] Kashiwagi T, Du F, Winey KI, Groth KM, Shields JR, Bellayer SP, et al. *Polymer* 2005;46:471–81.
- [12] Kashiwagi T, Grulke E, Hilding J, Groth K, Harris Jr RH, Shields JR, et al. *Polymer* 2004;45:4227–39.
- [13] Moniruzzaman M, Winey KI. *Macromolecules* 2006;39:5194–205.
- [14] Gilman JW, Jackson CL, Morgan AB, Harris Jr R, Manias E, Giannelis EP, et al. *Chem Mater* 2000;12:1866–73.
- [15] Gilman JW, Harris Jr RH, Shields JR, Kashiwagi T, Morgan AB. *Polym Adv Technol* 2006;17:263–71.
- [16] Jang BN, Wilkie CA. *Polymer* 2005;46:2933–42.
- [17] Jang BN, Wilkie CA. *Polymer* 2005;46:3264–74.
- [18] Costache MC, Jiang DD, Wilkie CA. *Polymer* 2005;46:6947–58.
- [19] Costache MC, Wang D, Heidecker MJ, Manias E, Wilkie CA. *Polym Adv Technol* 2006;17:272–80.
- [20] Jang BN, Jiang DD, Wilkie CA. *Polymer* 2005;46:9702–13.
- [21] Jang BN, Costache MC, Wilkie CA. *Polymer* 2005;46:10678–87.
- [22] Kuroki T, Honda T, Sekiguchi Y, Ogawa T, Sawaguchi T, Ikemura T. *Nippon Kagaku Kaishi* 1977;894–901.
- [23] Schroeder UKO, Ebert KH, Hamielec AW. *Makromol Chem* 1984;185:991–1001.
- [24] McNeill IC, Zulfiqar M, Kousar T. *Polym Degrad Stab* 1990;28:131–51.
- [25] Maurin MB, Dittert LW, Hussain AA. *Thermochim Acta* 1991;186:97–102.
- [26] McGrattan BJ. *Appl Spectrosc* 1994;48:1472–6.
- [27] Lattimer RP. *J Anal Appl Pyrolysis* 1995;31:203–25.
- [28] Jakab E, Omastova M. *J Anal Appl Pyrolysis* 2005;74:204–14.
- [29] Poutsma ML. *Macromolecules* 2003;36:8931–57.
- [30] Wang CA, Wang CC, Chen CY. *Polymer* 2005;46:5065–74.
- [31] Hadjiev VG, Iliev MN, Arepalli S, Nikolaev P, Files BS. *Appl Phys Lett* 2001;78:3193–5.
- [32] Zhang J, Jiang DD, Wilkie CA. *Polym Degrad Stab* 2006;91:641–8.
- [33] Wang ZM, Chung TC, Gilman JW, Manias E. *J Polym Sci Part B Polym Phys* 2003;41:3173–87.
- [34] Lewin M, Pearce EM, Levon K, Mey-Marom A, Zammarano M, Wilkie CA, et al. *Polym Adv Technol* 2006;17:226–34.
- [35] Chen K, Wilkie CA, Vyazovkin S. *J Phys Chem B*, submitted for publication. doi:10.1021/jp0759168.
- [36] Wilkie CA, McKinney MA. In: Troitzsch J, editor. *Plastics flammability handbook*. Munich: Hanser Publishers; 2004. p. 62.
- [37] Riva A, Zanetti M, Braglia M, Camino G, Falqui L. *Polym Degrad Stab* 2002;77:299–304.
- [38] Vaia RA, Jandt KD, Kramer EJ, Giannelis EP. *Chem Mater* 1996;8:2628–35.
- [39] Manias E, Chen H, Krishnamoorti R, Genzer J, Kramer EJ, Giannelis EP. *Macromolecules* 2000;33:7955–66.
- [40] Wilkie CA, Zheng X, Chigwada G, Costache M, Jang BN, Zhang J. In: Wilkie CA, Nelson GL, editors. *Fire and polymers IV: materials and concepts for hazard prevention*. Oxford University Press; 2006. p. 8–20.
- [41] Zhu J, Uhl FM, Morgan AB, Wilkie CA. *Chem Mater* 2001;13:4649.
- [42] Zhang J, Gupta R, Wilkie CA. *Polymer* 2006;47:4537–43.
- [43] Kashiwagi T, Gilman JW, Butler KM, Harris Jr RH, Shields JR, Asano A. *Fire Mater* 2000;24:277–89.
- [44] Kashiwagi T, Shields JR, Harris Jr RH, Davis RD. *J Appl Polym Sci* 2003;87:1541–53.
- [45] Kashiwagi T, Gilman JW. In: Grand AF, Wilkie CA, editors. *Flame retardancy of polymeric materials*. New York: Marcel Dekker; 2000. p. 353–89.